

Article

Experimental and Numerical Studies on the Traditional Penetration Mortise–Tenon Connection Reinforced by Self-Tapping Screws

Ting Guo ^{1,†} , Na Yang ^{1,*}, Haibin Zhou ^{2,†} and Shuangyong Wang ²¹ School of Civil Engineering, Beijing Jiaotong University, Beijing 100044, China; 16115319@bjtu.edu.cn² Research Institute of Wood Industry, Chinese Academy of Forestry, Beijing 100091, China; dvchow@126.com (H.Z.); tzlswsy@163.com (S.W.)

* Correspondence: nyang@bjtu.edu.cn

† These authors contributed equally to this work.

Abstract: In this paper, the mechanical performance improvement of traditional penetration mortise–tenon (PMT) connections reinforced by self-tapping screws (STSs) were experimental and numerical studied. Four unreinforced penetration mortise–tenon connections and four STS-reinforced connections were experimentally investigated under monotonic and low-frequency cyclic loading. Besides, the numerical model of PMT connections reinforced by STSs with different diameters and yield strength were established and analyzed. Their failure modes, rotational stiffness, moment-resisting capacity, ductility, and seismic behavior were studied. The experimental results indicated that the STSs reinforcements could enhance the moment-resisting capacity of the penetration mortise–tenon connection. Compared with unreinforced connections, the initial stiffness of STS-reinforced connections increased by 75% with the moment-resisting capacity increasing by 69%, respectively. Furthermore, the STSs reinforcement method can effectively restrict the pull-out of tenon during the whole loading process. Numerical simulation results showed that the yield strength of STS has little effect on the moment-bearing behavior of the connection. The diameter of STS significantly influences the connection performance, and the diameter of 8 mm is suggested.

Keywords: penetration mortise–tenon connection; Chinese fir; reinforcement; self-tapping screw; monotonic loading; cyclic loading; numerical simulation



Citation: Guo, T.; Yang, N.; Zhou, H.; Wang, S. Experimental and Numerical Studies on the Traditional Penetration Mortise–Tenon Connection Reinforced by Self-Tapping Screws. *Forests* **2022**, *13*, 513. <https://doi.org/10.3390/f13040513>

Academic Editor: Sofia Knapic

Received: 20 December 2021

Accepted: 13 January 2022

Published: 26 March 2022

Publisher's Note: MDPI stays neutral with regard to jurisdictional claims in published maps and institutional affiliations.



Copyright: © 2022 by the authors. Licensee MDPI, Basel, Switzerland. This article is an open access article distributed under the terms and conditions of the Creative Commons Attribution (CC BY) license (<https://creativecommons.org/licenses/by/4.0/>).

1. Introduction

Mortise–tenon (MT) connections are widely used in historical and traditional wooden structures in China and other Southeast Asian countries to connect beams and columns. Penetration mortise–tenon connections, featured by a beam without cross-sectional reduction inserted into a column with rectangular or circle section, is one of the most typical types of MT connections. Its construction is shown in Figure 1. The tensile-resisting capacity of the PMT connection mainly depends on the friction of the contact surfaces between the mortise and tenon and is very limited. Thus, tenon joints pulling out (Figure 2) and even completely separating from the mortise are prone to occur under axial loads, which severely weaken the integrity and safety of the wooden structure. In addition, the PMT connection can transmit moment by the wood compression perpendicular to grain and friction of the contacted surface between mortise and tenon joints under lateral loads such as seismic load [1]. However, due to manufacturing errors and wood shrinkage, there are often initial gaps between mortise and tenon, resulting in low initial rotational stiffness of the connection, which leads to connections being usually the weakest link in a wooden structure [2,3]. Therefore, it is important to restrict the tenon pull-out and improve the moment resistance behavior of PMTs for structural safety.

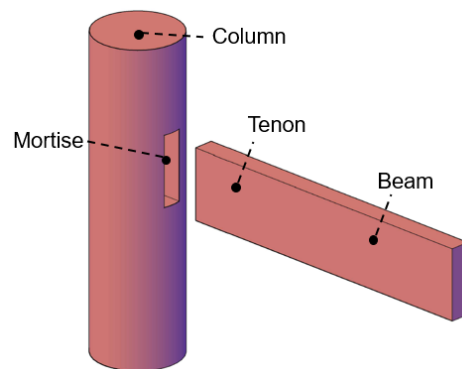


Figure 1. Penetration mortise–tenon connection.

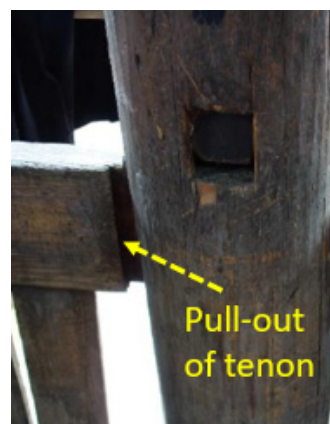


Figure 2. Pull-out of tenon [4].

Knowledge of the mechanical properties of PMT connections is necessary to enhance their moment resistance and limit the pulling out of the tenon. Thus far, some scholars have carried out many experimental tests, theoretical studies, and finite element analyses for PMT connections. Xu [5] carried out low-frequency cyclic loading on connections and found that the tenon pulling out was related to the controlled displacement of each loading cycle, but also to the number of cycles of the loading point on the connection. Considering the influence of initial gaps on the performance of PMT connections, Chang et al. [6,7] conducted monotonic loading tests on PMT connections used in the wooden structure in Taiwan and found that the initial gaps reduced the rotational stiffness of the connections. The Nuki connection used in Japan is similar to the PMT connections except for the existence of wedges for fasteners. Guan et al. [8] performed low-frequency reversed cyclic loading on Nuki connections and established the relationship of moment and rotation. They also studied the influence of oversize on the behavior of the Nuki connections. The 3D nonlinear finite element analysis indicated that the different oversize wedges introduced various tightness to the connection and proved that the wedges had significant effects on the racking resistance of the Nuki connection. Tanahashi et al. [9,10], Chang et al. [6], Xie et al. [11], and Yang et al. [12] established the theoretical model of the moment rotation relationship of PMT connections based on different assumptions. Briefly, the poor moment-resisting capacity and ease of pulling out of the tenon are the drawbacks of PMTs, which affects significantly the mechanical behavior of the whole structure.

To enhance the resisting capacity and limit the tenon pulling out of mortise–tenon connections, many methods of reinforcement have been proposed. Some scholars firstly suggested strengthening the PMT connection by installing flat steel on it. Xie et al. [13] conducted a low-frequency cyclic loading test on wooden frames characterized by MT connections strengthened with flat steel. The results indicated that flat steel reinforcement was suitable for hidden MT connection with obvious insufficient strength or stiffness.

However, Pan et al. [14] found that flat steel reinforcement would cause the redistribution of internal forces of members and increase the internal forces of some adjacent members while improving the rotational stiffness of connections. Improper reinforcement of flat steel may lead to the failure of other members. Some scholars [15,16] introduced more flexible fiber materials than flat steel as connection reinforcement. The tested results indicated that the CFRP reinforcement was an effective method to eliminate the tenon pulling out and improve the moment-resisting capacity as well as rotational stiffness. However, Yan et al. [17] carried out low-frequency cyclic loading tests on a scaled mortise–tenon wooden frame model and found that the CFRP reinforcement reduced the dissipated energy of the MT connections. Afterward, efforts to apply other reinforcement materials in MT connections such as metal dampers [14,18] and mild steel [19] were reported. However, most of these reinforcement methods need sufficient installation space and are not suitable for practical application. For real structures, infilled walls are often arranged near connections, and there is no sufficient operated and installed space for these reinforcements.

In this paper, an STS-reinforcing method was proposed for its convenient installation, low requirement of space, and cost efficiency. In addition, the performance improvement of PMT connections reinforced by STSs was evaluated by experimental and numerical studies. The failure modes, rotational stiffness and moment resistance capacity of connections were investigated. Besides, the influence of the STS parameters on the was analyzed. Based on the experimental and numerical investigation, a suggestion of a new STS-reinforced method was proposed and evaluated.

2. Experimental Program

To evaluate the reinforcing effect of STSs on the mechanical performance of PMT connections, two series of connections were fabricated—namely, unreinforced connections denoted as series U, and connections reinforced by self-tapping screws denoted as series S. All of the specimens had the same materials and same dimensions. There were four replicates in each series. Three of them were tested under monotonic loading, and the other one was tested under low-frequency cyclic loading. The information of all the tested PMT connection specimens is listed in Table 1.

Table 1. Information of tested specimens.

Series	Type of Connection	Specimen	Loading Method
U	Unstrengthened	U1	Monotonic
		U2	Monotonic
		U3	Monotonic
		U4	Cyclic
S	Self-tapping screws	S1	Monotonic
		S2	Monotonic
		S3	Monotonic
		S4	Cyclic

2.1. Materials

All of these wooden specimens were fabricated by Chinese fir (*Cunninghamia lanceolata*) from Guizhou Province in southeastern China. Columns were made of logs, and beams were made of plain sawn timber with a class grade of grade Ia according to GB50005-2003 *Code for Design of Timber Structures* [20]. The physical and mechanical properties were tested according to timber material test standard [21–25], as summarized in Table 2.

The partially threaded self-tapping screws were used as reinforcements in the STS-reinforced connections, with a length of 200 mm and a diameter of 6 mm.

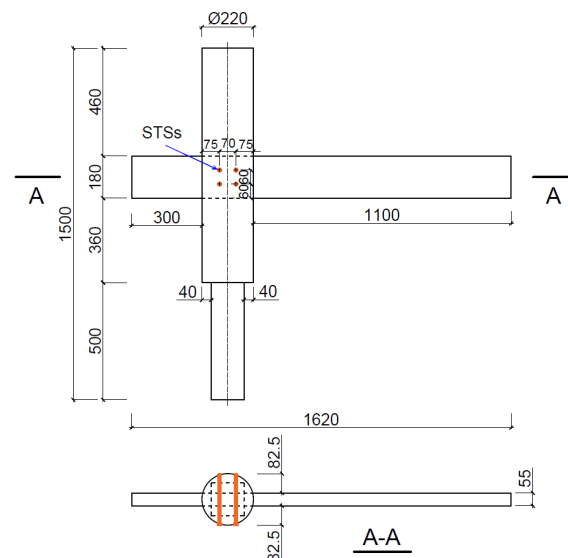
Table 2. Material properties of Chinese fir.

	<i>M.C</i>	ρ kg/m ³	f_t MPa	f_m MPa	E_m MPa	$f_{c,0}$ MPa	$f_{c,90,n}$ MPa
MV	9.03%	387	76.54	71.45	10192.50	48.68	4.68
COV	0.03	0.075	0.13	0.10	0.07	0.12	0.19

A total of 20 samples were used for each test. MV is the mean value, COV is the coefficient of variation. *M.C* is moisture content, ρ is density of wood, f_t is the tensile strength parallel to grain, f_m is the bending strength, E_m is the flexure modulus of elasticity, $f_{c,0}$ is the compressive strength parallel to grain, and $f_{c,90,n}$ is the compressive strength perpendicular to grain along radial direction.

2.2. Specimen Design

Based on the dimensions measured by the field survey, full-scale PMT connection specimens were fabricated. The details of the specimens are shown in Figure 3. The beam members were 180 mm × 55 mm in cross section and 1620 mm in length, and the column members were 220 mm in diameter and 1500 mm in length; the mortise on each column was 180 mm × 55 mm. Four STSs were arranged on each STS-reinforced connection, and the scheme is shown in Figure 3.

**Figure 3.** Specimen construction and dimension.

2.3. Loading Test Setup and Data Measurement

The test loading device is shown in Figure 4. The bottom end of the column was fixed to a steel beam by constraining its translation and rotation. The bottom end of the column was inserted into a U-shaped slot on the steel beam and pressed tightly by eight bolts. The steel beam was fixed to the floor by two anchor bolts. The top end of the column was applied a vertical load of 10 kN by jack1 with a loading capacity of 30 kN and a stroke range of 300 mm, to simulate the practical load. In the monotonic test loading, the vertical load leading to connection rotation was applied on the free end of the beam by Jack 2 with a loading capacity of 30 kN and a stroke range of 300 mm. Jack 2 was placed directly on the top face of the beam. In the low-frequency cyclic loading, the free end of the beam was connected to a vertically electro-hydraulic servo actuator through a hinge. The hydraulic actuator had a maximum loading capacity of 250 kN and a stroke range of 250 mm in two directions.

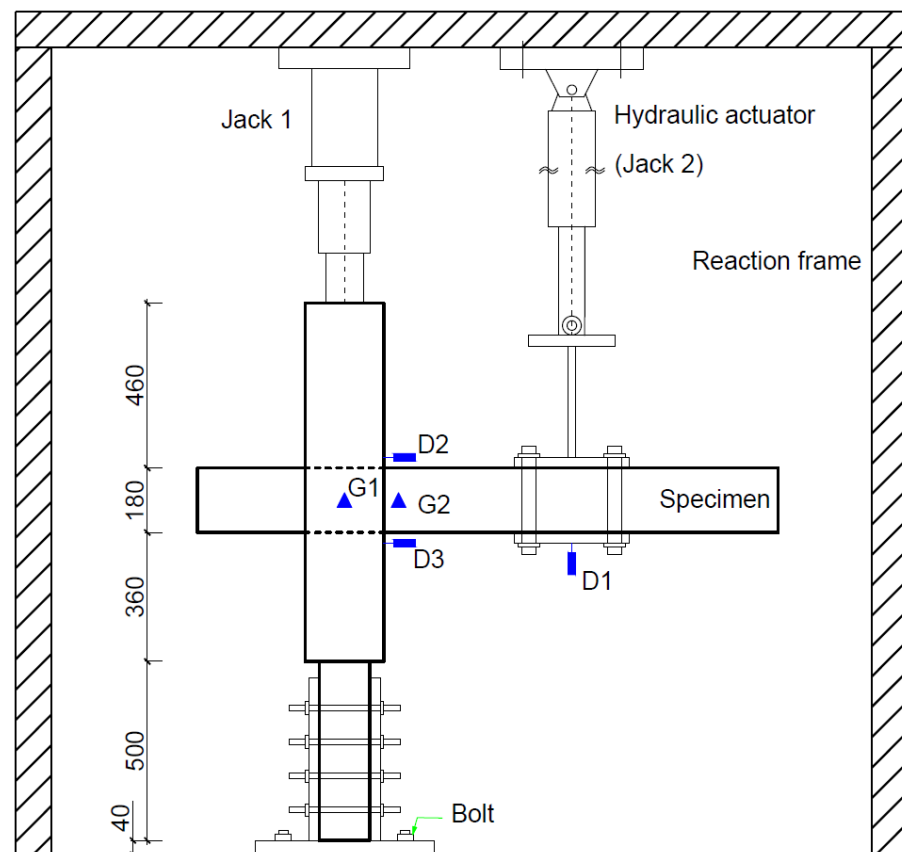


Figure 4. Loading test setup and sensor arrangement.

Three 200 mm range linear variable differential transformers (LVDTs) and two 30 deg range inclinometers were used to measure the displacement and rotation angle, respectively. The transducer arrangement is exhibited in Figure 4. Considering the rotation center is the center of the mortise, the moment applied to the connection can be calculated according to Equation (1).

$$M = F \times L \quad (1)$$

where F is the vertical force recorded by Jack 2 or hydraulic actuator; L is the horizontal distance between the loading point and the rotation center.

The rotation angle can be calculated according to Equation (2) or Equation (3). In order to obtain the pull-out amount of tenon, two displacement transducers (D_2 and D_3) were attached to the top and bottom surface of the beam to record the relative displacement between mortise and tenon. The pull-out value of tenon can be calculated according to Equation (4).

$$\theta = \frac{180}{\pi} \times \arctan \frac{D_1}{L} \quad (2)$$

$$\theta = G_2 - G_1 \quad (3)$$

$$\delta = \frac{D_2 + D_3}{2} \quad (4)$$

where D_1 is the vertical displacement of loading point measured by displacement transducer D_1 ; D_2 and D_3 are the displacements measured by displacement transducer D_2 and D_3 , respectively. G_1 and G_2 are the rotation angle of the beam and column, respectively. They are measured by inclinometers G_1 and G_2 , respectively.

2.4. Loading Program

The first step of the loading procedures in both the monotonic and cyclic tests was the application of an axial compression force with 10 kN on the top of the column, simulating roof load, which was kept constant during the whole test. In the subsequent loading steps, a vertical force was applied on the free end of the beam, generating a moment on the connection.

The monotonic loading tests were performed in control load and at each 4 kN increment. A cyclic test was performed in displacement-driven according to EN 12512 [26], as illustrated in Figure 5. θ_y is the yield rotation, which is determined by the monotonic test. The test program included one cycle in displacement $0.25\theta_y$ and $0.5\theta_y$, followed by three cycles in displacement $0.75\theta_y$, $1.00\theta_y$, $2.00\theta_y$, $4.00\theta_y$, etc. until the specimen failed. The vertical loading stopped under one of the following conditions: (1) the applied load dropped to 80% of the peak load; (2) the loading device reached its range, or the displacement and rotation measurement was out of range of the sensors; (3) the tested specimen failed.

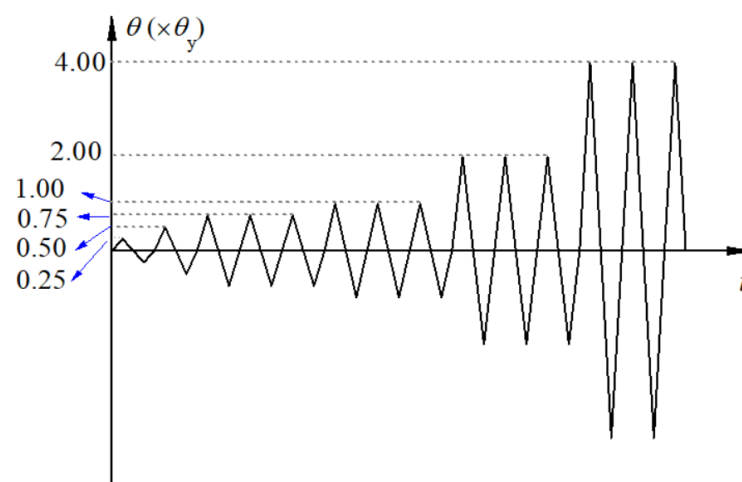
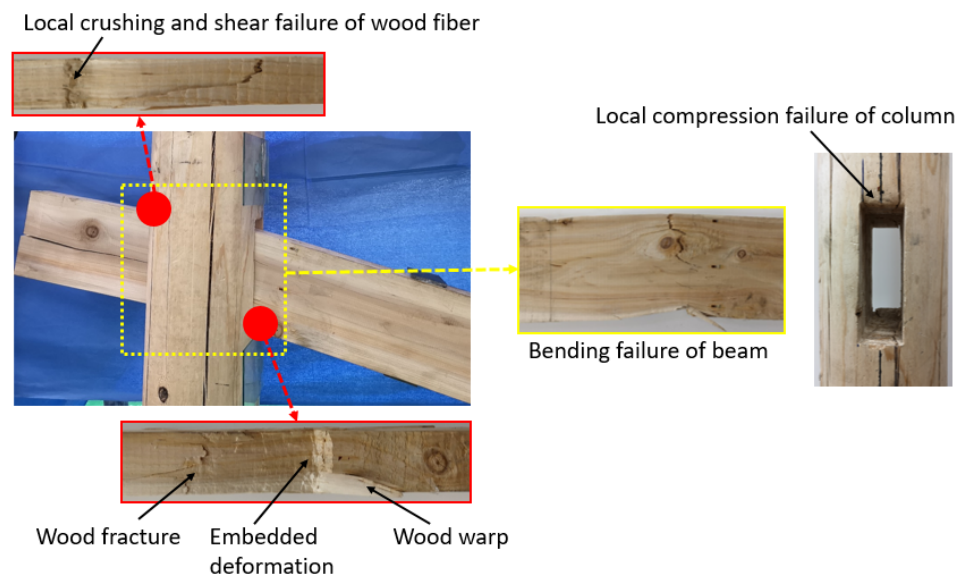


Figure 5. Loading scheme.

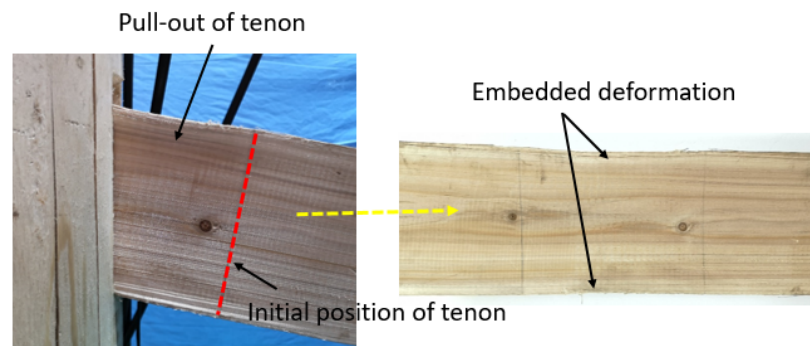
3. Experimental Observations and Failure Modes

3.1. Non-Reinforced Connections

Three unreinforced connection replicates under monotonic loading suffered similar damage. During the whole loading test, they successively experienced tenon rotation, contact extrusion, the gradual intensification of tenon and mortise, and increasingly severe, embedded plastic deformation until the bending failure of the beam member. In the later stage of loading, the wood fiber fracture at the embedded zone and wood fiber warp was also observed. The failure modes of unreinforced penetration mortise–tenon connections under monotonic loading and cyclic are given in Figure 6. The failure mainly occurred on beam members, severe local crushing, fracture, and shear failure of wood fiber at the tenon zone contacted to mortise due to the embedded compression perpendicular to grain and shear. For specimens U1 and U3, the beam failure occurred at the inclined section formed by connecting the top and bottom embedded areas of the tenon. In particular, for specimen U2, due to the presence of knots, the surface wood fibers near the knot were broken firstly and then prorated to the bottom compression side near the contact area between mortise and tenon (Figure 6a). Moreover, the beam end of specimen U2 split along the initial crack. Compared with severe damage of beam element, the columns of all three specimens were subjected to only slight damage, as shown in Figure 6a. The column was subjected to local compression failure due to stress concentration and slight plastic deformation parallel to grain when in contact with the tenon.



(a) Monotonic loading (U2)



(b) Cyclic loading (U4)

Figure 6. Failure modes of unreinforced connection (Series U).

Permanently embedded deformation perpendicular to grain was also observed in connection specimen under low-frequency reversed cyclic loading (Figure 6b). However, compared with that of specimens under monotonic loading, the deformation of the specimen under cyclic loading was much smaller, which was caused by a continuous change in the contact area of tenon and mortise due to pull-out of the tenon. Eventually, the connection specimen U4 failed with pulling out of the tenon.

3.2. Reinforced Connections

For the STS-reinforced connections, the initial slight compressive deformation perpendicular to grain under monotonic loading also occurred at later than that of unreinforced connections, and at the rotation around 3.7° (mean value of series S). Moreover, the pulling out of the tenon occurred at unreinforced connections was restricted in STS-reinforced connections.

The failure mode of STS-reinforced connections under monotonic loading is shown in Figure 7. As can be seen, the excessive compressive deformation perpendicular to grain presented in unreinforced connections was significantly reduced due to the reinforcement of self-tapping screws. It should be noted that screws 1 and 2 near the vertical loading point on the end of the beam were bent slightly, and screws 3 and 4 away from the vertical loading point were not bent in connection specimen S1, under monotonic loading. This was because the local compression applied on screws 1 and 2 was larger than screws 3 and 4.

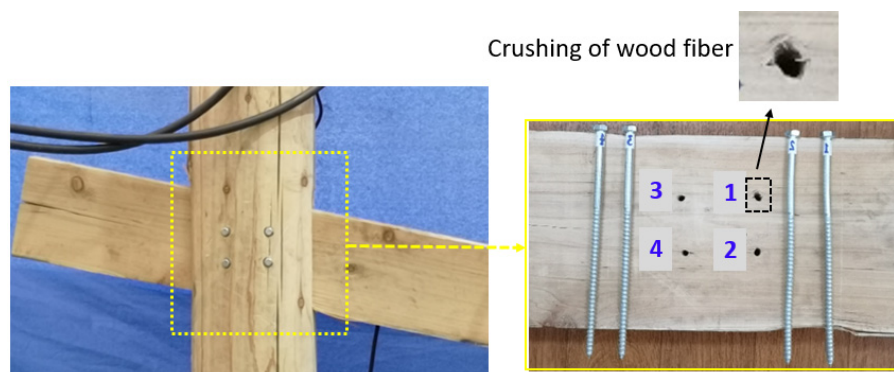


Figure 7. Failure mode of STS-reinforced connection under monotonic loading (series S).

As demonstrated in Figure 8, the vertical load and moment were generated at the connection when the vertical load was applied at the free end of the beam. Under the action of moment M , the connection rotated around the geometric center of the four self-tapping screws, and wood around the holes subjected to the forces F_1 , F_2 , F_3 , and F_4 , respectively. Under the action of vertical force F , the wood around the holes was subjected to the force F_v . Thus, the total forces F_{Ti} (i represents 1, 2, 3, and 4) acted on each dowel hole were obtained, as illustrated in Figure 8. The total force acted on dowel holes 1 and 2 was greater than holes 3 and 4. Therefore, the crushing of wood fiber around holes 1 and 2 was more severe than that around the other two holes. In addition, there were compressed force $F_{t,c}$ and friction force $F_{t,f}$ acting on the tenon top surface, compressed force $F_{b,c}$, and friction force $F_{b,f}$ acting on the tenon bottom surface, respectively. The PMT connections reinforced by STSs rely on the embedded compression and friction of tenon surface contacting with mortise but also the local compression of wood fiber surrounding STSs.

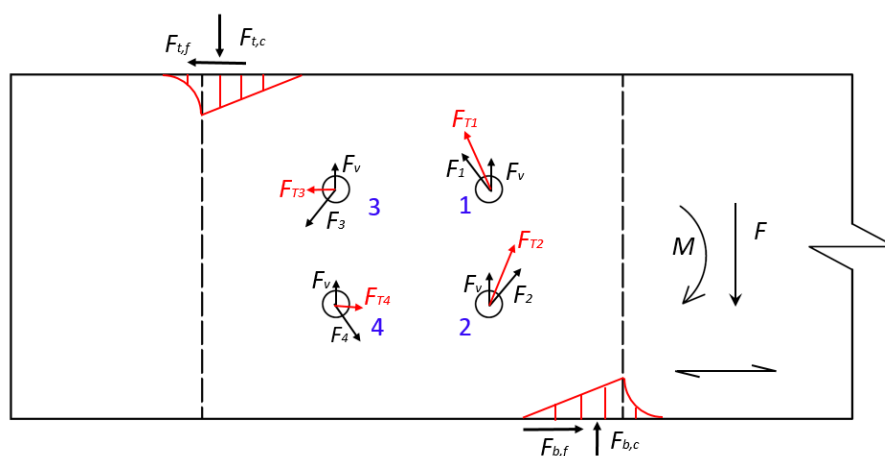


Figure 8. Forces on the tenon of STS-reinforced connections under monotonic loading.

Under cyclic loading, the pulling out of the tenon of STT-reinforced connections was restricted due to the presence of STSs. The plastic embedded deformation of the tenon, as well as combined bending and shear deformation of the STSs, were also observed. The connection specimen S4 failed early by beam fracture due to the presence of knots on the tenon top surface.

4. Experimental Results Analysis

Figure 9 demonstrates the moment–rotation (M – θ) curves of the two series of PMT connection specimens under monotonic loading. It can be seen that the unreinforced connections display an almost linear relationship between moment and rotation during the initial loading phase, then show a nonlinear relationship with decreasing slope after the

compression perpendicular to grain deformation occurred. The moment–rotation curves of all the three self-tapping screw-reinforced connections display a small slope before the rotation around 2°, then exhibit an almost linear relationship with a larger slope, and then also show a nonlinear relationship with decreasing slope. This was because there were initial gaps between mortise and tenon in the connections, which led to a small rotational stiffness before the mortise and tenon contact with each other. With the increasing rotation, tenon came in contact with mortise, and the connection stiffness increased. After the tenon was pressed into the mortise and plastic compressive deformation perpendicular to grain occurred, the moment-rotation curve became nonlinear.

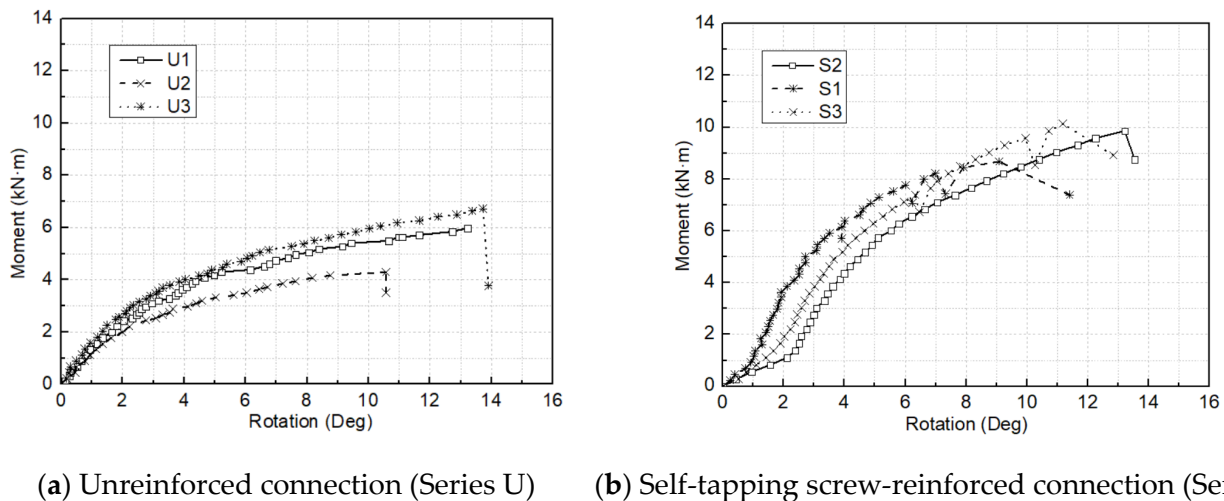


Figure 9. Moment–rotation curves under monotonic loading.

The initial stiffness K_{ini} , yield rotation θ_y , yield moment M_y , maximum moment-resisting capacity M_{max} , failure rotation θ_u , and ductility μ of the two series under monotonic loading are summarized in Table 3. The initial stiffness and yield point of connection specimens were determined according to EN 12512 [26]. From Figure 10, the yield values are determined by the intersection between the two lines of the moment–rotation curves. The maximum moment-resisting capacity was the moment corresponding to the peak point. The failure rotation corresponded to the point at which the moment of the specimen dropped to 80% of the maximum moment. The ductility is defined as $\mu = \theta_u/\theta_y$. As can be seen in Table 3, the initial stiffness and maximum moment-resisting capacity of unreinforced connections are 1.00~1.37 kN·m/° and 4.30~6.72 kN·m, respectively. The unreinforced connections had the lowest initial stiffness and maximum moment-resisting capacity, which indicated that the self-tapping-screw-reinforced method can improve the initial stiffness and moment-resisting capacity of PMT connections. Figure 11 shows normalized parameters of the unreinforced connection specimens and other derived parameters on the structural performance of connections. Compared with that of unreinforced connection (U), the initial stiffness of self-tapping screw connections (S) increased by 75% with the moment-resisting capacity increasing by 69%, respectively. In terms of ductility, the unreinforced connection specimens have the largest deformation ratio of 4.62, which implies that the unreinforced connection performed well in deformation. Even though the deformation ratio of self-tapping screw-reinforced connection specimens are lower than that of unreinforced connections, the deformation ratios are also higher than 3.38, which indicates well deformation capacity of this kind of reinforced connection [27].

Table 3. Monotonic test results of connection specimens.

Type of Connection	Specimen	K_{ini}	θ_y	M_y	θ_u	M_{max}	μ
		(kN·m/°)	(°)	(kN·m)	(°)	(kN·m)	($\mu = \theta_u/\theta_y$)
Unstrengthened	U1	1.22	2.90	3.58	13.23	5.98	4.56
	U2	1.00	2.53	2.62	10.57	4.30	4.18
	U3	1.37	2.68	3.82	13.73	6.72	5.13
	Mean	1.20	2.70	3.34	12.51	5.66	4.62
	Cov	0.16	0.07	0.19	0.14	0.22	0.10
Self-tapping screws	S1	2.46	2.78	5.51	11.40	8.67	4.10
	S2	1.79	4.85	5.99	13.54	9.86	2.79
	S3	2.05	3.96	5.82	12.84	10.13	3.24
	Mean	2.10	3.87	5.77	12.59	9.56	3.38
	Cov	0.16	0.27	0.04	0.09	0.08	0.20

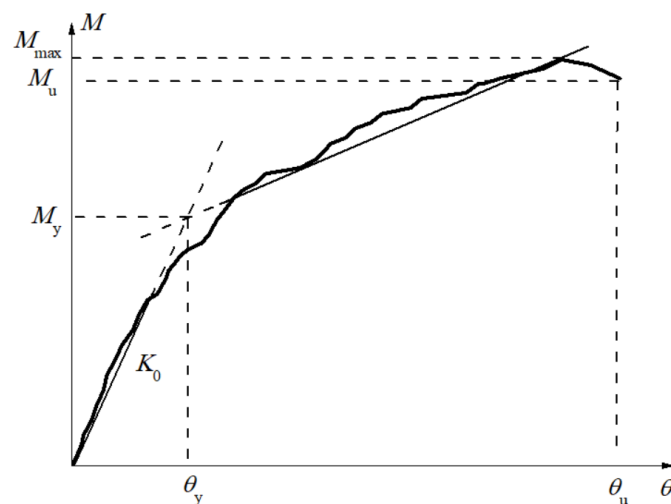
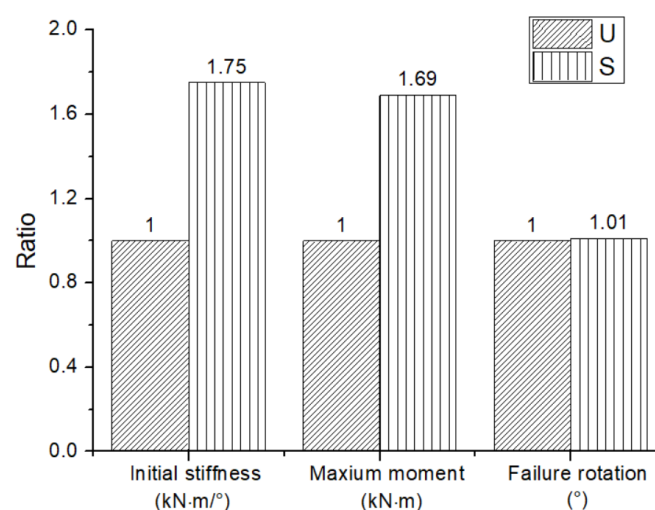
**Figure 10.** Parameters definition of moment–rotation curves of connections.**Figure 11.** Normalized parameters of PMT connections under monotonic loading.

Figure 12 shows the pulling out of the tenon of unreinforced connection specimen U4 under cyclic loading. It can be found that the pull-out amount gradually increased with the increase in rotation. Finally, the pull-out amount reached 144.5 mm. The pull-out amount of the STS-reinforced connection specimen S4 was 7.9 mm. This indicated that the

STS reinforcement method can effectively restrict the pull-out of tenon during the whole loading process.

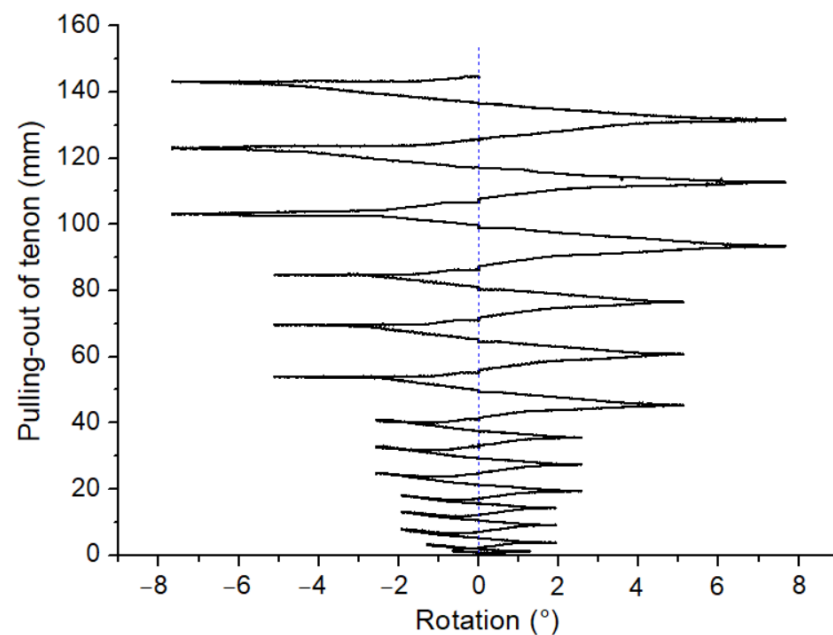


Figure 12. Pulling out of the tenon of unreinforced connection U4.

5. Numerical Simulation

To obtain stress (strain) distribution within the PMT connection reinforced by STSs and investigating the influence of STSs parameters on the initial rotational stiffness of this connection, 3-D nonlinear finite element models of the connection were developed using the commercial code ABAQUS.

5.1. Finite Element Modeling

The Specimen S1 serves as a reference for finite element models. The construction and dimension of the beam are the same as that of specimen S1. The bottom end of the column of specimen S1 is inserted into the U-shaped slot on the steel beam fixed with the ground. Therefore, this part can be regarded as a fixed constraint. The column is modeled as 1000 mm in height and 220 mm in diameter. The initial gap of 2 mm between mortise and tenon in specimen S1 is also considered in the numerical model. Thus, the tenon of this model is 184 mm in height and 55 mm in width. In addition, four partial threaded STSs are simplified as plain round screws with the same diameter and length of the specimen.

Two materials are used for the connections. Columns and beams are made of wood, and STSs are made of steel. In the numerical simulation, wood is defined as an orthotropic material. The same modulus of elasticity is used for wood in tension and compression. The elastic modulus and yield strength of the wood are adopted based on the tested results (Table 2). The values of Poisson coefficients V_{LR} , V_{LT} , V_{RT} are 0.45, 0.51, 0.36, respectively. Steel is defined as isotropic elasto-perfectly plastic materials both in tension and compression. The elastic modulus and Poisson coefficient of steel are 2.1×10^5 MPa and 0.3, respectively. The yield strength of the steel of the reference model is 240 MPa.

Three-dimensional linear reduced integral solid element C3D8R is adopted for the finite element model. The grid size of critical parts of this model is about 10 mm, and that of other parts is about 20 mm or 30 mm. Figure 13 shows the mesh generation of the connection.

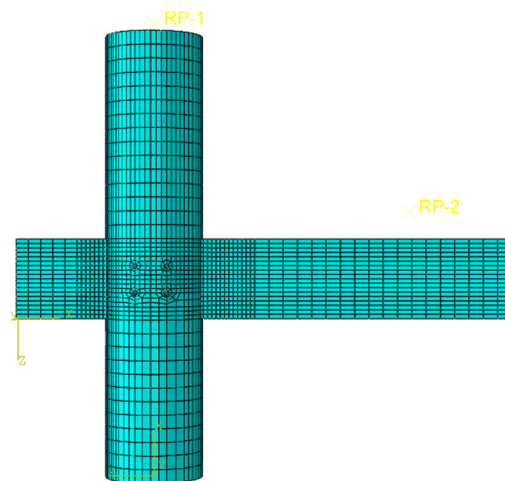


Figure 13. Numerical model of PMT connection reinforced by STSs.

During the beam rotating, there is a slide between surfaces in contact. Contact can occur in the interface between beam and column, STS and beam, STS and column. In the normal direction of the contact interface, the “hard” contact model is used to describe the relationship between the normal contact pressure and the gap (the distance between the two surfaces). When the gap between two surfaces is zero, the two surfaces are subject to contact constraints, and the contact pressure can be transferred between the contact surfaces. When the two surfaces are separated, the contact gap is greater than zero, the constraint between the contact surfaces is released, and the contact pressure is zero.

Contact causes friction in the tangent direction of the contact interface. The friction is simulated using the Coulomb stick-slip model. The friction coefficient between wood and wood is set equal to 0.35, the friction coefficient between STSs and wood is set equal to 0.3.

The boundary conditions of the numerical model are consistent with that of the tested connection specimen. The column bottom is fixedly connected. Reference point RP-1 is established above the center of the column top and coupled with the top surface of the column. A concentrated vertical load of 10 kN is applied to this reference point. Reference point RP-2 is established and coupled to the loading area of the top surface of the beam. A downward vertical load is applied to this reference point in the same way as in the test.

5.2. Comparison of Numerical and Experimental Results

Figure 14 shows the moment-rotation curves of specimen S1 and the finite element model. It can be seen that the curves of the two coincide in the gap stage. When tenon and mortise contact and press tightly, the rotational stiffness of the two increases suddenly. However, the finite element model is stiffer than specimen S1 due to the non-consideration of the initial cracks, knots, and other defects presented in specimen S1 in the finite element model. Specimen S1 finally shows a load drop stage, while the finite element model does not experience load drop due to without simulating wood failure. Generally, the shape and trend of the two curves are basically the same when the rotation angle is within eight degrees. Table 4 shows the comparison of the rotational stiffness and moment-bearing capacity. K_0 is rotational stiffness in the gap stage. K_{ini} and M_{max} are the same definitions in Section 4. The numerical result of M_{max} is in good agreement with experimental observations. The numerical model is stiffer than the test specimen, but the relative error is within 15%, which indicates that the 3D-FEM model can predict well the stiffness and moment-bearing capacity of the PMT connection reinforced by STSs. Figure 15 shows the beam deformation of the numerical model. It is observed that the embedment deformation on the contact area between mortise and tenon.

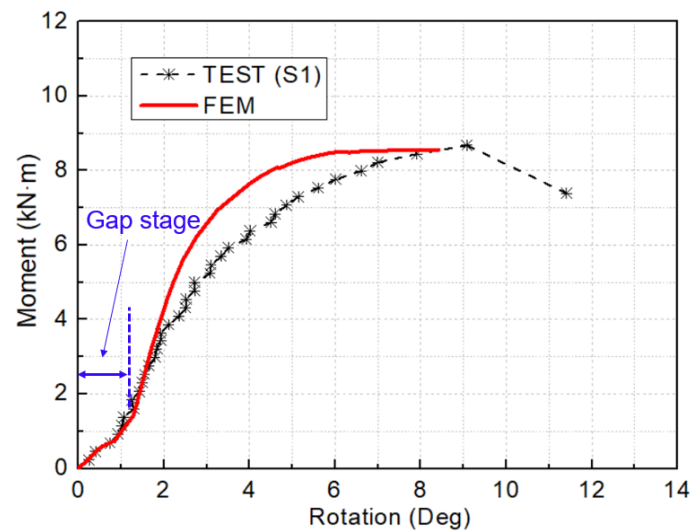


Figure 14. Comparison between numerical and experimental M- θ curves of PMT connections reinforced by STSs.

Table 4. Comparison of numerical and test results.

	K_0 (kN·m/°)	K_{ini} (kN·m/°)	M_{max} (kN·m)
S1	0.99	2.46	8.67
FEM	1.10	2.84	8.55
Relative error	11%	15%	−1%

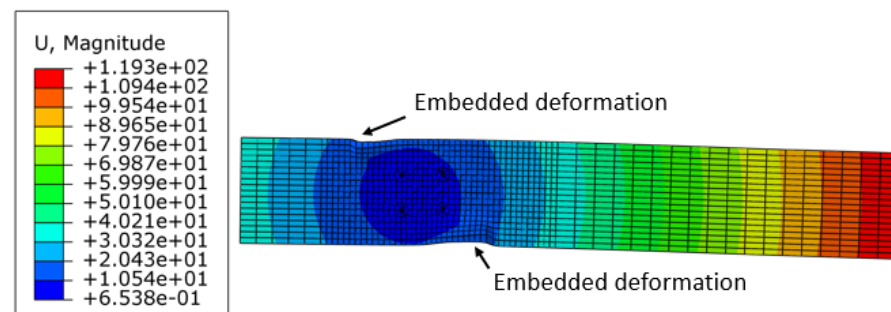


Figure 15. Deformation of PMT connections reinforced by STSs.

5.3. Influence of the STSs

5.3.1. Strength

To investigate the yield strength (f_y) of STS on load-bearing behavior of PMT connection reinforced by STSs. Four finite element models with yield strength ranging between 240 MPa and 600 MPa have been modeled. Figure 16a shows the moment-rotation relationship of connection with different yielding strengths of STS. It can be seen that the moment-rotation curves of the four models have the almost same rotational stiffness and moment-resisting capacity. Figure 16b shows the normalized parameters of the numerical reference model and other derived parameters on the structural performance of other numerical models. The ratio is between 1.00 and 1.09, which indicates that the yield strength of STS has little effect on the moment-bearing behavior of the PMT connection reinforced by STSs.

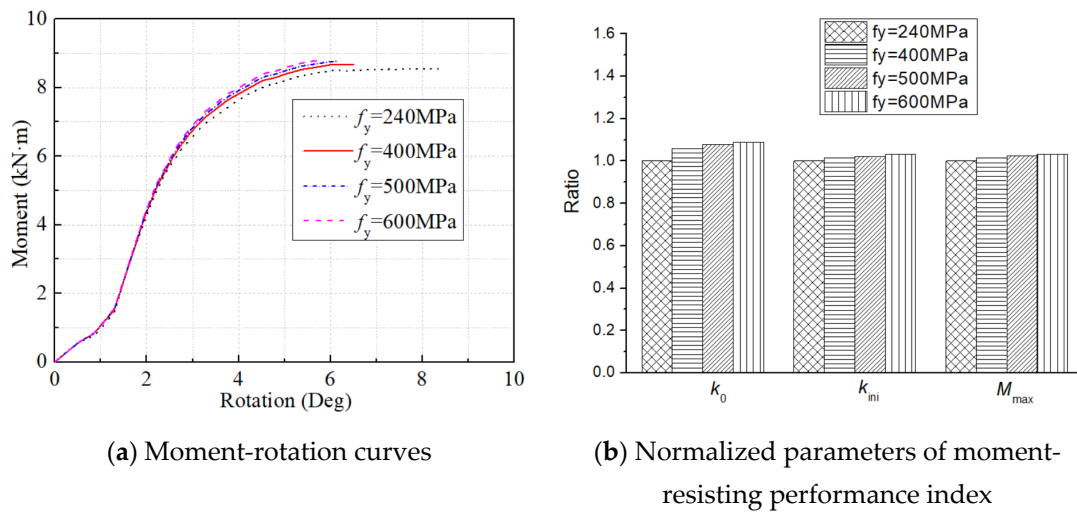


Figure 16. Influence of the yield strength of STSs.

5.3.2. Diameter

To evaluate the diameter of STS on the load-bearing behavior of PMT connections reinforced by STSs, three PMT connections reinforced by STSs of diameter ranging between 6 and 10 mm have been modeled. Figure 17 shows the influence of the diameter of STS on connection. As STS diameter increases, the rotational stiffness in the gap stage increases slightly. The initial rotational stiffness and maximum moment of the numerical model with STS diameter of 8 mm and 10 mm are greater than that of the numerical model with STS diameter of 6 mm. The moment-rotation curves of numerical model with STS diameter of 8 mm is almost the same with that of numerical model with STS diameter of 10 mm. It indicates that the rotational stiffness and moment-bearing capacity of the connection increase with the increase of STS diameter ranging from 6 mm to 10 mm. However, when the diameter reaches 8 mm, the improvement is limited. The STS with a diameter of 8 mm is suggested to be adopted as the reinforcement.

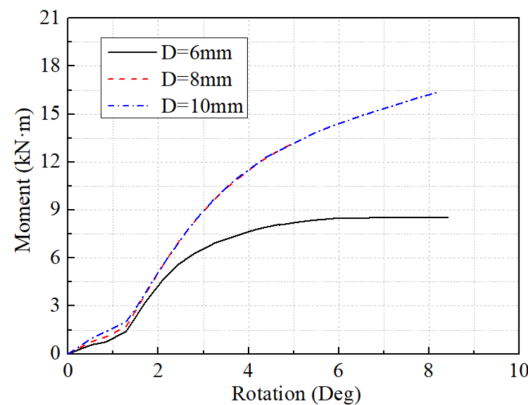


Figure 17. Influence of the diameter of STSs.

6. Conclusions

This paper presented the test results of two series (unreinforced and self-tapping-screw-reinforced) of full-scale traditional penetration mortise–tenon connections. The damage characteristics, failure modes, initial rotational stiffness and moment-resisting capacity of all the connections are investigated. The influence of diameter and yield strength of STS on the moment-bearing behavior of the connection is discussed. The main conclusions are as follows:

- (1) The unreinforced penetration mortise–tenon connections failed by the beam fracture under monotonic loading and the pull-out of tenon under cyclic loading;
- (2) The self-tapping-screw-reinforced method significantly improved the initial stiffness and moment-resisting capacity of unreinforced connections. The self-tapping-screw reinforcements could restrict the pull-out of the tenon during the whole loading process;
- (3) The yield strength of STS has little effect on the moment-bearing behavior of the connection. The diameter of STS significantly influences the connection performance, and the diameter of 8 mm is suggested;
- (4) The self-tapping-screw-reinforced methods have the advantages of cost effectiveness, easy implementation, and low demand for installation space. It is a reasonable reinforced method.

Author Contributions: Conceptualization, methodology, investigation, writing—original draft, data curation, T.G.; conceptualization, methodology, investigation, resources, supervision, funding acquisition, N.Y.; conceptualization, investigation, writing—review and editing, resources, funding acquisition, project administration, H.Z.; investigation, validation, S.W. All authors have read and agreed to the published version of the manuscript.

Funding: This research was funded by the National Key Research and Development Program of China (No.2018YFD0600303), National Natural Science Foundation of China (General Program) (No.51778045), National Key Research and Development Program of China (No. 2018YFC0705600), and 111 Project of China from Ministry of Education and the Bureau of Foreign Expert of China (No.B13002).

Data Availability Statement: Not applicable.

Acknowledgments: This work was financially supported by the National Key Research and Development Program of China (No.2018YFD0600303), National Natural Science Foundation of China (General Program) (No.51778045), National Key Research and Development Program of China (No. 2018YFC0705600), and 111 Project of China from Ministry of Education and the Bureau of Foreign Expert of China (No.B13002).

Conflicts of Interest: The authors declare no conflict of interest.

References

1. Wu, G.; Gong, M.; Gong, Y.; Ren, H.; Zhong, Y. Mechanical performance of mortise and tenon joints pre-reinforced with slot-in bamboo scrimber plates. *J. Wood Sci.* **2019**, *65*, 38. [[CrossRef](#)]
2. Leijten, A.J.M.; Brandon, D. Advances in moment transferring dwv reinforced timber connections—Analysis and experimental verification, Part 1. *Constr. Build. Mater.* **2013**, *43*, 614–622. [[CrossRef](#)]
3. Brandon, D.; Leijten, A.J.M. Advances in moment transferring dwv reinforced timber connections—Numerical analyses and verification, Part 2. *Constr. Build. Mater.* **2014**, *56*, 32–43. [[CrossRef](#)]
4. Ling, L.J. *Investigation on the Current Situation and Study on Safety Improvement Technology of through Type Timber Frame Dwellings—Taking Bapa Village of Qiandongnan as an Example*; Xi’an University of Architecture and Technology: Xi’an, China, 2018. (In Chinese)
5. Xu, M.G. *Study of Aseismic Behavior of Mortise-Tenon Joints in Chinese Ancient Timber Buildings*; Southeast University: Nanjing, China, 2011. (In Chinese)
6. Chang, W.-S.; Hsu, M.-F.; Komatsu, K. Rotational performance of traditional Nuki joints with gap I: Theory and verification. *J. Wood Sci.* **2006**, *52*, 58–62. [[CrossRef](#)]
7. Chang, W.-S.; Hsu, M.-F. Rotational performance of traditional Nuki joints with gap II: The behavior of butted Nuki joint and its comparison with continuous Nuki joint. *J. Wood Sci.* **2007**, *53*, 401–407. [[CrossRef](#)]
8. Guan, Z.W.; Kitamori, A.; Komatsu, K. Experimental study and finite element modelling of Japanese “Nuki” joints—Part two: Racking resistance subjected to different wedge configurations. *Eng. Struct.* **2008**, *30*, 2041–2049. [[CrossRef](#)]
9. Tanahashi, H.; Suzuki, Y. *Basic Concept and General Formulation of Restoring Force Characteristics of Traditional Wooden Joints*; WCTE; Curran Associates, Inc.: Auckland, New Zealand, 2012; pp. 378–387.
10. Tanahashi, H.; Suzuki, Y. Seismic reinforcement of traditional timber structures by ladder type frames. *Disaster Mitig. Cult. Herit. Hist. Cities* **2008**, *2*, 171–178.
11. Xie, Q.; Wang, L.; Zheng, P.; Zheng, P.; Zhang, L.; Qian, C. Theoretical analysis on moment-rotation relationship of straight mortise-tenon joints for Chinese traditional wooden buildings. *J. Hunan Univ. (Nat. Sci.)* **2017**, *44*, 111–117. (In Chinese)
12. Yang, Q.; Yu, P.; Law, S.-S. Load resisting mechanism of the mortise-tenon connection with gaps under in-plane forces and moments. *Eng. Struct.* **2020**, *219*, 110755. [[CrossRef](#)]

13. Xie, Q.F.; Zhao, H.T.; Xue, J.Y.; Yao, K.; Sui, Y. An experimental study on the strengthening of mortise-tenon joints in ancient Chinese wooden buildings. *China Civ. Eng. J.* **2008**, *41*, 28–34. (In Chinese)
14. Pan, Y.; Wang, C.; Tang, L.N. Comparative research on flat steel and damper strengthening of straight type of tenon-mortise joints. *J. Southwest Jiaotong Univ.* **2014**, *49*, 981–986, 1031. (In Chinese)
15. Xu, M.; Qiu, H. Experimental study on seismic behavior of mortise-tenon joints in Chinese ancient timber buildings. *J. Build. Struct.* **2012**, *33* (Suppl. S2), 345–349. (In Chinese)
16. Chen, C.-J. *The Study on Improved Mechanical Properties of Reinforced Traditional Chuan-Dou Timber Joints in Taiwan*; Urban Development and Architecture of National University of Kaohsiung: Kaohsiung, Taiwan, 2016.
17. Yan, W.M.; Zhang, B.; Zhou, Q.; Guo, Y. Aseismic strengthening experiments on Chinese ancient tenon-mortise joints. *Earthq. Resist. Eng. Retrofit.* **2011**, *33*, 89–95. (In Chinese)
18. Wang, C. *Study of Mechanics Model and Seismic Strengthening of Tenon-Mortise Joints in Chinese Ancient Timber Structure*; Southwest Jiaotong University: Chengdu, China, 2012. (In Chinese)
19. Lu, W.D.; Deng, D.L. Experimental research on seismic performance of wooden mortise-tenon joints before and after reinforcement. *J. Earthq. Eng. Eng. Vib.* **2012**, *32*, 109–116. (In Chinese)
20. GB5000 5–2003; Code for Design of Timber Structures. Ministry of Construction of the People’s Republic of China: Beijing, China, 2003. (In Chinese)
21. GB 193 5–2009; Method of Testing in Compressive Strength Parallel to Grain of Wood. Standardization Administration of China: Beijing, China, 2009. (In Chinese)
22. GB 1936. 1–2009; Method of Testing in Bending Strength of Wood. Standardization Administration of China: Beijing, China, 2009. (In Chinese)
23. GB 1936. 2–2009; Method for Determination of the Modulus of Elasticity in Static Bending of Wood. Standardization Administration of China: Beijing, China, 2009. (In Chinese)
24. GB 193 8–2009; Method of Testing in Tensile Strength Parallel to Grain of Wood. Standardization Administration of China: Beijing, China, 2009. (In Chinese)
25. GB 193 9–2009; Method of Testing in Compression Perpendicular to Grain of Wood. Standardization Administration of China: Beijing, China, 2009. (In Chinese)
26. EN12512; Timber Structures-Test Methods-Cyclic Testing of Joints Made with Mechanical Fasteners. European Committee for Standardization (CEN): Brussels, Belgium, 2005.
27. Blaß, H.J.; Schädle, P. Ductility aspects of reinforced and non-reinforced timber joints. *Eng. Struct.* **2011**, *33*, 3018–3026. [[CrossRef](#)]